submitted for publication in the Proceedings of the 27th International SAMPE Technical Conference, Albuquerque, NM, October 9-12, 1995

CHARACTERIZING AND MODELING ORGANIC BINDER BURNOUT FROM GREEN CERAMIC COMPACTS

K. G. Ewsuk, J. Cesarano III , R. J. Cochran, B. F. Blackwell, and D. R. Adkins
Sandia National Laboratories, Albuquerque, NM 87185-1349

ABSTRACT

New characterization and computational techniques have been developed to evaluate and simulate binder burnout from pressed powder compacts. Using engineering data and a control volume finite element method (CVFEM) thermal model, a nominally one dimensional (1-D) furnace has been designed to test, refine, and validate computer models that simulate binder burnout assuming a 1-D thermal gradient across the ceramic body during heating. Experimentally, 1-D radial heat flow was achieved using a rod-shaped heater that directly heats the inside surface of a stack of ceramic annuli surrounded by thermal insulation. The computational modeling effort focused on producing a macroscopic model for binder burnout based on continuum approaches to heat and mass conservation for porous media. Two increasingly complex models have been developed that predict the temperature and mass of a porous powder compact as a function of time during binder burnout. The more complex model also predicts the pressure within a powder compact during binder burnout. Model predictions are in reasonably good agreement with experimental data on binder burnout from a 57-65% relative density pressed powder compact of a 94 wt% alumina body containing ~3 wt% binder. In conjunction with the detailed experimental data from the prototype binder burnout furnace, the models have also proven useful for conducting parametric studies to elucidate critical material property data required to support model development.

KEY WORDS: Model, Binder Burnout, Ceramic

1. INTRODUCTION

The properties and performance of a ceramic component are determined by a combination of the materials from which it was fabricated and its processing history. Most ceramic components are manufactured by shape forming a powder/binder system using a mechanical or isostatic press. [1-6] The organic binder in the system provides plasticity for shaping, and green compact strength for handling. [7-9] Removal of the organic binder from the powder compact after pressing and before sintering is acritical step in ceramic component manufacturing. Generally, the organic binder is removed from (i.e., burned-out) of a ceramic compact by thermal decomposition, which occurs by dissociation and/or pyrolysis. [5-6, 10-11] Organic decomposition produces gaseous by-products that can result in pressure build-up within the ceramic part. To avoid developing internal pressures that can damage or destroy

the pressed part, gas pressure build-up within the ceramic body must be controlled during burnout; therefore, the organics must be removed gradually, when the permeability of the body is highest, and prior to densification and pore closure. Heating rate, temperature, and time are the key process parameters. Empirical approaches are generally used to design the burnout time-temperature cycle, often resulting in high development costs, excessive processing times and energy usage, and higher overall manufacturing costs. Ideally, binder burnout should be completed as quickly as possible without damaging the compact, while using a minimum of energy. Computational process modeling offers one means to achieve this end [12-14].

The objective of this study was to develop characterization techniques and experimentally validated computer models that can be used to better understand, control, and optimize binder burnout from green ceramic compacts formed by dry pressing. A combination of quantitative experimental analysis and computational modeling was used to understand the complex phenomena associated with the burnout of organic binder from a powder compact. Experimentally, this entailed utilizing conventional characterization methods, such as thermogravimetric analysis (TGA), as well as developing a new technique to quantitatively describe binder burnout. The experimental effort played the critical role of providing the scientific foundation necessary to support model development. The ultimate goal of the computational modeling effort is to provide engineering level accuracy on inexpensive computer platforms with minimum analysis turnaround times for process design parametric studies.

2. EXPERIMENTAL

This study focused on characterizing binder burnout in a typical ceramic compact formed by dry pressing. A representative, 94 wt% alumina body was chosen for study, and a combination of conventional and novel characterization techniques were used to characterize the powder and the compacts formed with the powder. Binder burnout experiments were conducted in a specially designed furnace to determine the effects of heating rate, and pressed powder compact density on burnout. Additionally, data from the binder burnout experiments was used to conduct parametric studies to support model development, and for model validation.

2.1 Materials and Forming Binder burnout experiments were conducted on pressed powder compacts of a spray-dried 94 wt% Al_2O_3 powder[1] containing 3 wt% of a 50/50 mixture (by weight) of methylcellulose and hydroxypropylcellulose binder. Ceramic annuli of approximately 6.7 cm outside diameter, 2.0 cm inside diameter, and 1.3 cm tall were formed by uniaxial pressing ~ 100 g of powder in a 7.4 x 2.2 cm stainless steel die cavity, followed by isostatic pressing. Die pressing pressures of 4.4 and 8.9 MPa were used in combination with isostatic pressing pressures of 35.4 and 1782.5 MPa to produce ~57 and ~65% relative density compacts for testing, respectively.

2.2 Prototype Binder Burnout Furnace To support the computational modeling effort, a nominally one-dimensional (1-D) heat and mass transfer experiment was designed using engineering data and a two-dimensional (2-D) axisymmetric control volume finite element method (CVFEM) thermal model to predict transient heat flow [15] . Experimentally, 1-D radial heat flow was achieved using a rod-shaped heater that directly heats the inside surface of a stack of six ceramic annuli surrounded by low thermal conductivity thermal insulation[2]

---

1 94ND2, Martin Marietta Specialty Components, Largo Fl 34649-2908

2 Wacker WDS, Zircar Products Inc., Florida, NY 19021

DISCLAIMER

DISCLAIMER

Portions of this document may be illegible in electronic image products. Images are produced from the best available original document.

(Figure 1a). To minimize axial temperature gradients in the ceramic stack (Figure 1b), annuli of low thermal conductivity zirconia insulation[3] were placed on the top and bottom of the Al_2O_3 ceramic stack, and the Al_2O_3 annuli in contact with the zirconia were pre-calcined (i.e., the binder was burned out before the experiment). Heating element temperature uniformity was ensured with a 24 gauge nichrome wire[4] heating element wound on a 1.27 cm diameter alumina tube[5] with sixteen threads per inch machined into it[6]. To ensure thermocouple temperature accuracy, potential cross-talk from stray electromagnetic radiation was minimized by using a heating element designed with two parallel threads (e.g., like a striped barber pole) with the nichrome wire going up one parallel thread and down the other to complete the ~10 cm long heating zone. High sensitivity, 0.0127 cm diameter Type E thermocouples,[7] strategically positioned in the ceramic stack, were used to monitor radial and axial temperature changes during heating. Mass loss and CO_2 emissions due to binder decomposition were monitored continuously during burnout using a computer interfaced balance[8] and a CO_2 analyzer[9], respectively. A computer[10] controlled data acquisition system[11] was used to control power input to the furnace through a 200 W power supply[12]. The data acquisition system also recorded time-dependent temperature, mass loss, and CO_2 emissions during binder burnout. (Some of the initial data was collected using a first generation system[13])

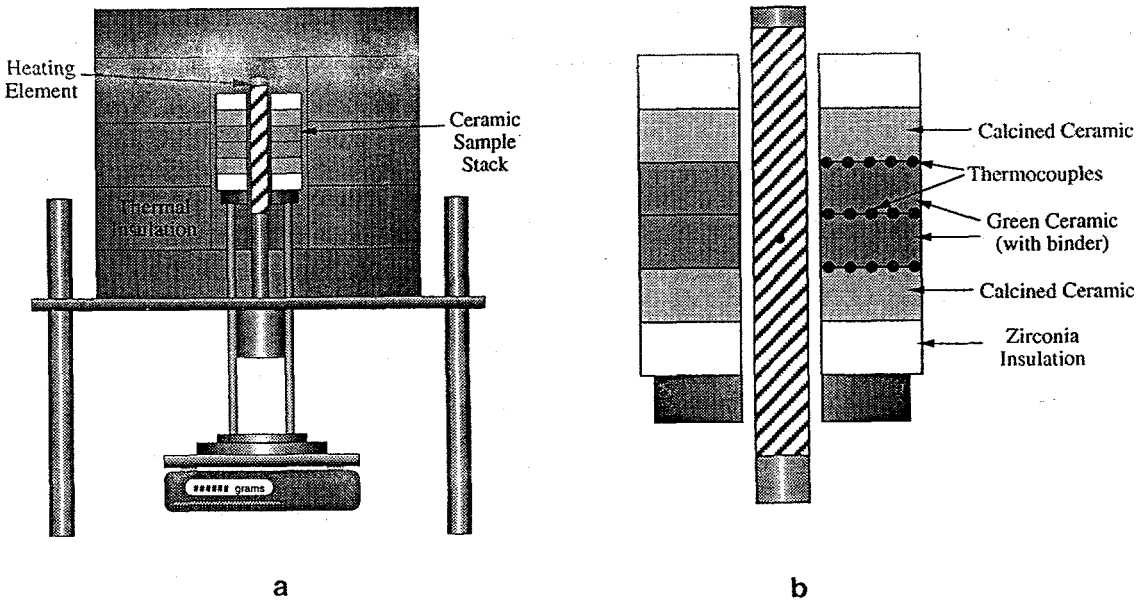

Figure 1 Cross section of: a) the prototype binder burnout furnace designed to simulate 1-D radial heat flow to characterize binder burnout and support model development; and b) the ceramic annuli stack configuration used in the furnace during burnout experiments to ensure 1-D radial heat flow and minimize axial temperature gradients. Radii reported in the text are from the centerline of the furnace heating element, where r = 0.00 cm is the center of the furnace and the heater, and r = 0.96 ± 0.1 cm and r = 3.33 ± 0.1 cm are the inside and outside diameters of the ceramic compact annuli stack, respectively.

---

3 ZYZ3, Zircar Products Inc., Florida, NY 19021
4 Ni80/Cr20, Omega Technologies Company, Stamford, CT 06906
5 AD-998, Coors Ceramic Co. (Ceramicon Designs), Golden CO, 80403
6 Machined Ceramics, Bowling Green, KY 42101
7 chromel-constantan, Omega Technologies Company, Stamford, CT 06906
8 BB2400 balance with GA37 D-A Converter, Mettler Instrument Corp., Highstown, NJ 08520
9 CEA 244 Infrared Analyzer, CEA instruments, Inc., Emerson, NJ 07630
10 Power Macintosh 8100/10 AV, Apple Computer Co., Cupertino, CA 95014
11 Lab View Version 3.1 with NIDAQ 6.0, National Instruments Corp., Austin, TX 78730-5039
12 HP 6034A, Hewlett Packard Corp., Palo Alto, CA 94304
13 4310-08-01, Acromag, Wixom, MI (with an IBM compatible PC, using a Variac power supply)

2.3 Materials Characterization To determine the mass loss during thermal decomposition, TGA experiments were conducted on the spray-dried alumina powder using a commercial thermal analysis system[14]. Heating rates of 2.5, 5, and 10°C/min from room temperature to 900°C in ~20 ml/min flowing Ar or air were examined.

The true or theoretical density of the as-received, green alumina powder (i.e., with binder) and the calcined powder (i.e., after heating to ≥900°C to decompose the organic binders and salt precursor additives) was determined by helium pycnometry[15]. Bulk density after pressing was determined from the measured mass and dimensions of the powder compact. Relative density was determined by normalizing the measured bulk density to the theoretical density of the green or calcined powder, as applicable.

The temperature dependent emissivity, heat capacity, and thermal conductivity of the green and calcined alumina powder compacts were either estimated on the basis of handbook data [16], or determined by conducting parametric studies. Estimates of both emissivity and thermal conductivity were used in the CVFEM model predictions to compare to heat flow data obtained from the experiments conducted in the prototype binder burnout furnace at 30 and 50W constant power. The temperature dependent thermal conductivity of green and calcined pressed powder compacts was estimated from the measured radial transient heat flow in the ceramic stack during binder burnout experiments.

The permeability of green and calcined powder compacts was determined using a liquid penetration technique [17]. In-house equipment was designed and constructed to measure the volume of (liquid) methanol that permeates a 2.5×10^{-6} m^2 cross sectional area of a disk-shaped specimen under a pressure of 3898 Pa. Measurements were made on ~57% relative density green and ~52% relative density calcined disks, 2.54 cm diameter and ~0.15 cm thick formed by die-pressing at 51.8 MPa.

2.4 Binder Burnout Experiments Experiments to evaluate time-dependent temperature (within a ceramic stack), mass loss, and CO_2 emissions during binder burnout were conducted in the prototype binder burnout furnace. To accurately monitor transient heat flow in the ceramic stack during binder burnout, up to nineteen different thermocouples were strategically positioned within the furnace during any given experiment. To determine the effects of pressing density variations on binder burnout, experiments were conducted on 57 and 65% theoretical density ceramic annuli stacked four high in the prototype furnace. By controlling the rate of power input from 0.2 and 2.0 W/min to the furnace heater, the effects of heating rate on binder burnout were also examined.

3. BINDER BURNOUT MODEL DEVELOPMENT

The computational modeling effort centered on producing a macroscopic model of the burnout process. Model development was based on continuum approaches to heat and mass conservation for porous media [18]. In the as-pressed form, the green compact is initially a 40-50% (by volume) porous body that is impermeable to gas flow. During calcining (i.e., binder burnout) the porous powder compact becomes permeable. The binder burnout process involves decomposition and combustion of the cellulose components that make up the binder. This process results in a heat and mass transfer problem involving both mass diffusion and convection processes in a porous matrix. The thermal decomposition of the binder was modeled using a set of increasingly complex computational models, including a: 1) no-flow;

14 TGA 7, Perkin Elmer, Norwalk, CT 06856-9966
15. Ultrapycnometer 1000, Quantachrome Corp., Syosset, NY 11791

2) lumped-gas flow; and 3) multi-component-gas flow model. With increasing complexity additional computer time is required to complete the analysis; however for all of cases presented, 1-D flow computations can be performed on a desktop PC.

3.1 No-Flow Model The no-flow model is based on the transient, energy conservation equation for a solid. This consists of energy storage, conduction, and energy source terms:

$$\rho c \frac{\partial T}{\partial t} = \nabla \cdot (k \nabla T) + \dot{m}'''_b \Delta H \qquad (1)$$

The energy source term represents the energy release of the exothermic combustion reaction of the cellulose binder. Utilizing TGA data, a two-component Arrhenius reaction model was developed to predict the mass loss of binder as a function of temperature:

$$\dot{m}'''_b = \rho_b \varepsilon_{b_o} \left(\sum_{i=1}^{2} - \alpha_i \exp(-\beta_i / T) u_i^{\gamma_i} \right) \qquad (2)$$

The Arrhenius model, and the two individual components, u_1 and u_2, of the model are shown in comparison to the TGA data in Figure 2. The mass loss term was used with an assumed heat of reaction for binder combustion to provide the magnitude of the energy source term as a function of time and temperature as shown in Equation (1). The no-flow model predicts the temperature and mass of a green powder compact as a function of time during binder burnout.

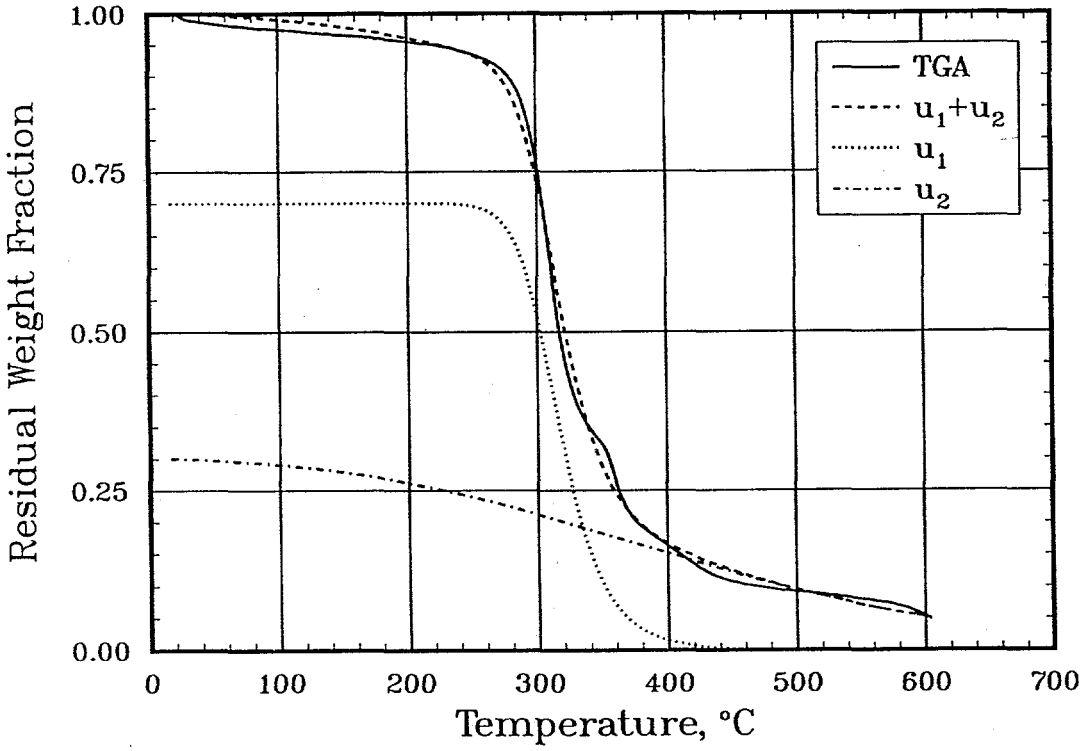

Figure 2. The temperature dependent, two-component Arrhenius reaction model used to approximate mass loss and drive the energy source term in the computer models during binder burnout. The individual components, u_1 and u_2, and the measured (TGA) mass loss data for heating in Ar at 2.5°C/min are also shown for comparison.

3.2 Lumped-Gas Flow Model To account for the flow of air into the powder compact, and the counter-flow of combustion by-products out of the compact during binder burnout, the lumped-gas flow model introduces two porous flow, mass conservation equations for ambient air and binder gas, and a momentum conservation law for porous flow. Additionally the model adds convection to the energy conservation equation. The two mass conservation equations for air and binder gas are:

$$\varphi \frac{\partial}{\partial t}(\rho_{air}) + u \cdot \nabla (\rho_{air}) = 0 \quad and \quad \varphi \frac{\partial}{\partial t}(\rho_{bg}) + u \cdot \nabla (\rho_{bg}) = \varphi \dot{m}'''_{bg} \tag{3}$$

The binder gas is assumed to be the sum of the by-products of fully combusted binder. Mass diffusion of the two gas components are ignored in the mass conservation equations. Momentum conservation is modeled using Darcy's law for laminar, incompressible fluid flow in a porous media:

$$u = -\frac{K}{\mu} \nabla P \tag{4}$$

The permeability is assumed to vary linearly as a function of residual mass fraction of binder present in the compact. Pressure within the compact during binder burnout is calculated using the ideal gas law. Convection is added to the energy conservation equation to account for the gas flow in the porous matrix:

$$(\rho c)_m \frac{\partial T}{\partial t} + (\rho c)_f u \cdot \nabla T = \nabla \cdot (k_m \nabla T) + \dot{m}'''_{bg} \Delta H \tag{5}$$

The lumped-gas flow model adds the transient prediction of pressure inside the pressed powder compact, along with the concentration of the ambient air and binder gas in the porous matrix.

3.3 Multi-Component Gas Flow Model More accurate predictions of the pressure within a pressed powder compact during binder burnout will ultimately be achieved using a multi-component-gas flow model. This model will introduce mass conservation equations for the atmospheric (i.e., air) reaction gas components and the individual gas by-product components of binder combustion. A simplified multi-component diffusion model will be used for the gas phase diffusion process in the mass transport model. This model will introduce diffusion processes to examine the movement of oxygen present in the ambient environment, into the reaction zone within the sample. Additionally, the chemical reactions associated with binder burnout will be used to consider more complex reactions, including incomplete reaction by-products in the binder gas during burnout.

4. RESULTS AND DISCUSSION

4.1 Prototype Binder Burnout Furnace Measured and predicted temperature profiles in a stack of ~65% relative density ceramic annuli after heating for 120 min with 30 W power are presented in Figure 3. The spatial temperature variations predicted using the 2-D axisymmetric CVFEM thermal model are in reasonably good agreement with the temperatures measured at select positions within the ceramic stack. Both model and experiment indicate that, as desired, relatively uniform radial heat flow is achieved in the prototype binder burnout furnace. Additionally, as designed, there is minimal temperature variation axially through the green ceramic components. The reasonably good agreement between model and

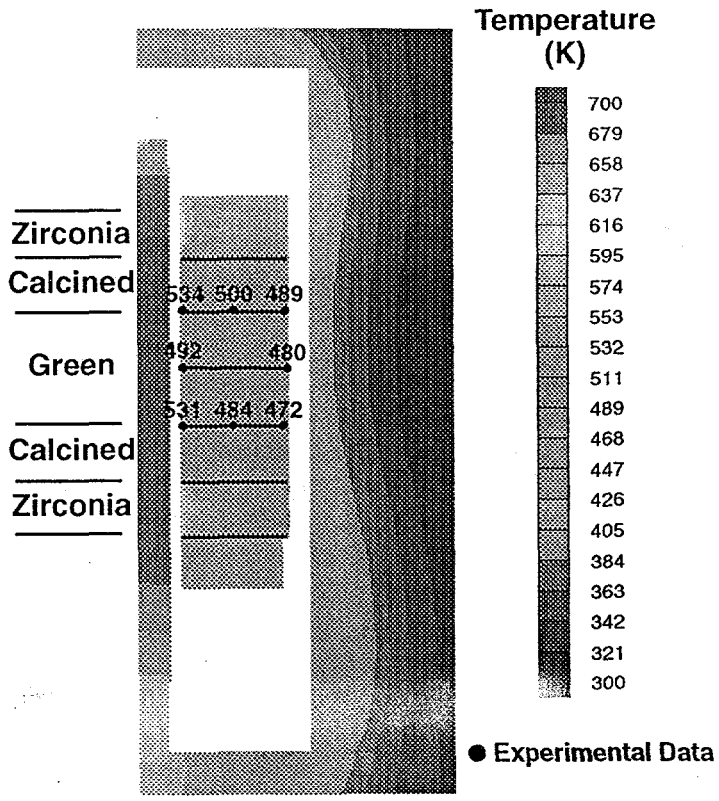

Figure 3. The measure and predicted temperature profiles in a ceramic stack after heating for 120 min with 30 W power. There is good agreement between experiment and model predictions, and uniform radial heat flow was achieved in the prototype binder burnout furnace.

experiment was achieved using estimates of the powder compact emissivity and thermal conductivity in the model calculations. Better agreement can be anticipated by tuning these two variables to better reflect the actual properties of the ceramic compacts being tested. Likewise, the CVFEM thermal mode has potential use to conduct parametric studies to support binder burnout model development. For example, it is possible to use the model to estimate the emissivity and thermal conductivity of a ceramic material by tuning the model parameters to replicate the observed spatial temperature variations.

4.2 Materials Characterization A representative TGA mass loss curve for as-received alumina powder heated in Ar at 2.5°C/min is shown in Figure 2. Similar curves were obtained in both flowing Ar and air, and with heating rates of 2.5, 5, and 10°C/min. Burning out in air or with slower heating rates shifts the mass loss curve to slightly lower temperatures, but the same general results are observed. In general, the cellulose binder starts to decompose at just above 200°C, and most of the binder is burned out between 200 and 400°C.

From pycnometry measurements, the theoretical density of the as-received alumina powder (with binder) and the calcined powder (after binder burnout) was determined to be 3535 and 3844 kg/m^3, respectively.

From liquid penetration experiments, it was determined that the as-pressed, green powder compacts (with binder) are impermeable to methanol. The compacts become permeable during binder burnout. A permeability of 2×10^{-6} m^2 was measure for the calcined powder

compact. This value is in good agreement with representative values for porous powder compacts reported in the literature. [18]

4.3 Binder Burnout Experiments In general, results from the experiments conducted in the prototype binder burnout furnace are very detailed, precise, and highly reproducible. Figure 4 shows representative results from a typical experiment conducted in the prototype binder burnout furnace. Time dependent changes in power, temperature, mass, and CO_2 emissions are monitored during binder burnout. Results show that there is strong thermal coupling between the heater and the ceramic stack. This coupling makes it possible to infer temperatures in the ceramic stack from measured heater temperatures to ensure run to run reproducibility. One of the benefits of this reproducibility is that, for more accurate mass loss measurements, a separate mass loss experiment can be conducted under identical thermal conditions without thermocouples in the ceramic stack.

In a typical binder burnout experiment, the hottest part of the furnace is the heating element, followed by the inner and then outer diameters of the ceramic stack (see Figure 4). The time dependent temperature gradient across the radius of the ceramic stack can be accurately measured, and can be used to calculate the temperature dependent thermal conductivity of the ceramic. The temperature gradient increases with time, and ultimately stabilizes at longer times (e.g., >180 min in Figure 4) after binder burnout is complete. The exothermic binder burnout reaction, which is temperature activated, initiates at the hotter, inner diameter of the ceramic stack at ~60 minutes, and the temperature gradient across the ceramic stack clearly increases at this time. At the same time, a distinct decrease in binder mass and increase in CO_2 emissions occurs. There is also a distinct difference in the rate of temperature rise in

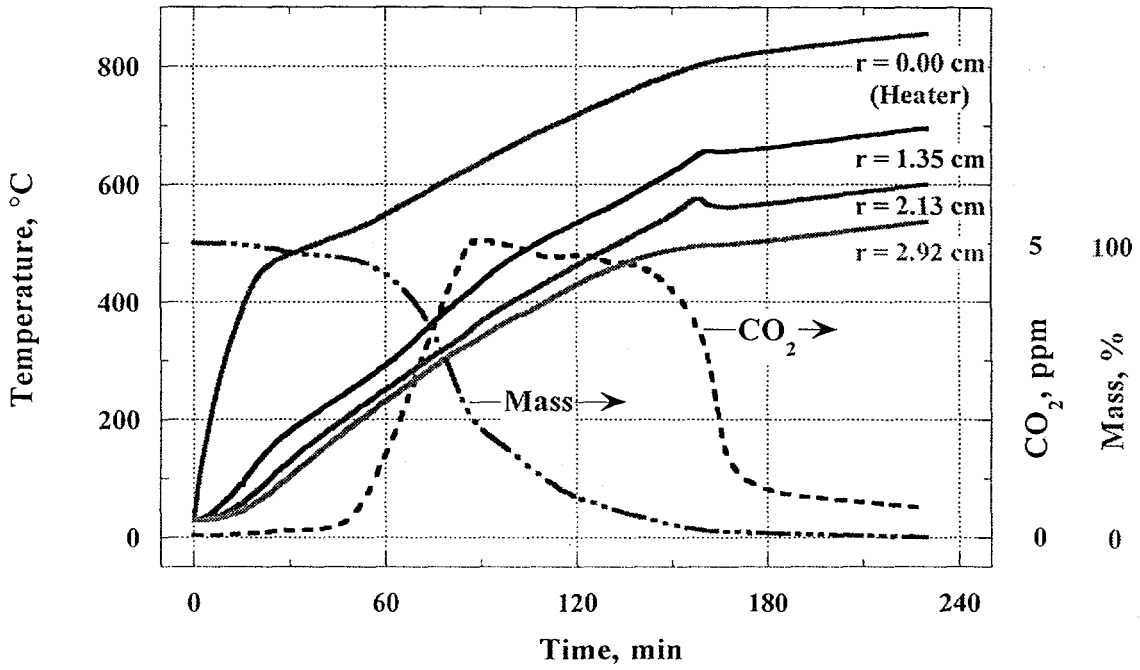

Figure 4. Results from a typical experiment conducted in the prototype binder burnout furnace. The heating profile was produced by increasing the power from 25 to 60 W at 2 W/min, followed holding at 60 W constant power for ~200 min. Time dependent changes in heater temperature, in the temperature of the ceramic compact temperature at radial positions of r = 1.35, 2.13, and 2.92 cm (in the center of the stack), and in binder mass and CO_2 emissions during binder burnout are shown.

the powder compact before and after binder burnout. When the organic binder is present and the ceramic compact is impermeable to fluid flow, the temperature increase with time is nearly four times greater than after binder burnout is complete, and the ceramic powder compact is permeable.

Binder burnout results support the general belief that the rate of temperature increase with time during binder burnout is a critical processing parameter. Heating with 2 W/min versus 0.2 W/min power increase from 25 to 60 W produced faster heating rates, larger temperature gradients through the ceramic stack, and cracking of individual ceramic annuli during binder burnout.

Pressed powder compact density differences between 57 and 65% relative density appear to have no significant effect on binder burnout, indicating that the density variations common in pressed ceramic components can be ignored in the binder burnout process.

4.4 Model Predictions The no-flow model is the simplest computational model developed in this study. It predicts the temperature and mass of a green powder compact as a function of time, but assumes that there is no gas flow into or out of the powder compact during binder burnout. The lumped gas flow model is slightly more sophisticated in that it also accounts for pressure driven gas flow into and out of a powder compact under the influence of pressure gradients created by gas volume expansion during heat-up, and by the evolution of gas by-products from the burnout reaction. While the "no-flow" assumption is unrealistic, in comparison to experimental data, the no-flow model makes a reasonably good first order approximation of binder mass loss from, and transient heat flow through, a porous powder compact during binder burnout (Figures 5 and 6). The predicted changes in the residual weight fraction of binder with time from the no-flow model show a sigmoidal-shaped curve similar to that obtained experimentally, with comparable absolute changes in mass with time (Figure 5). By incorporating gas flow into the analysis, the predictions of the lumped-gas flow model show even better agreement (Figure 5).

Time dependent temperatures predicted by the no-flow model at radial positions of 1.81 and 2.99 cm between the two green samples in the ceramic stack also show good agreement with experimental data (Figure 6). For the example presented in Figure 6, excellent agreement between model and experiment is observed at short times (i.e., < 120 min), but the model slightly overestimates the temperature at longer times (i.e., >240 minutes). Predictions from the lumped-gas flow model also showed good agreement with experimental binder burnout data, although this model slightly underestimates temperature during the intermediary times (i.e., from 120 - 240 min).

Based on the agreement between the model predictions and the experimentally measured transient heat flow through pressed ceramic powder compacts, parametric studies were conducted to determine the thermal conductivity of the green and calcined alumina powder compacts. This was accomplished by tuning the thermal conductivity used in the model calculations to produce model predictions that replicate the transient heat flow determined experimentally. Low thermal conductivities were determined for both the green and calcined powder compacts, but the green body has a slightly higher thermal conductivity (Table 1). The low thermal conductivity is expected for a porous ceramic body. The higher thermal conductivity for the green powder compact is attributed to the presence of the organic binder in that body, and to the slightly higher physical connectivity from binder-ceramic contacts.

In addition to predicting time dependent changes in mass and temperature, the lumped-gas flow model also can predict time dependent pressure within a powder compact during binder burnout. Typical results presented in Figure 7 indicate two peak pressures develop during

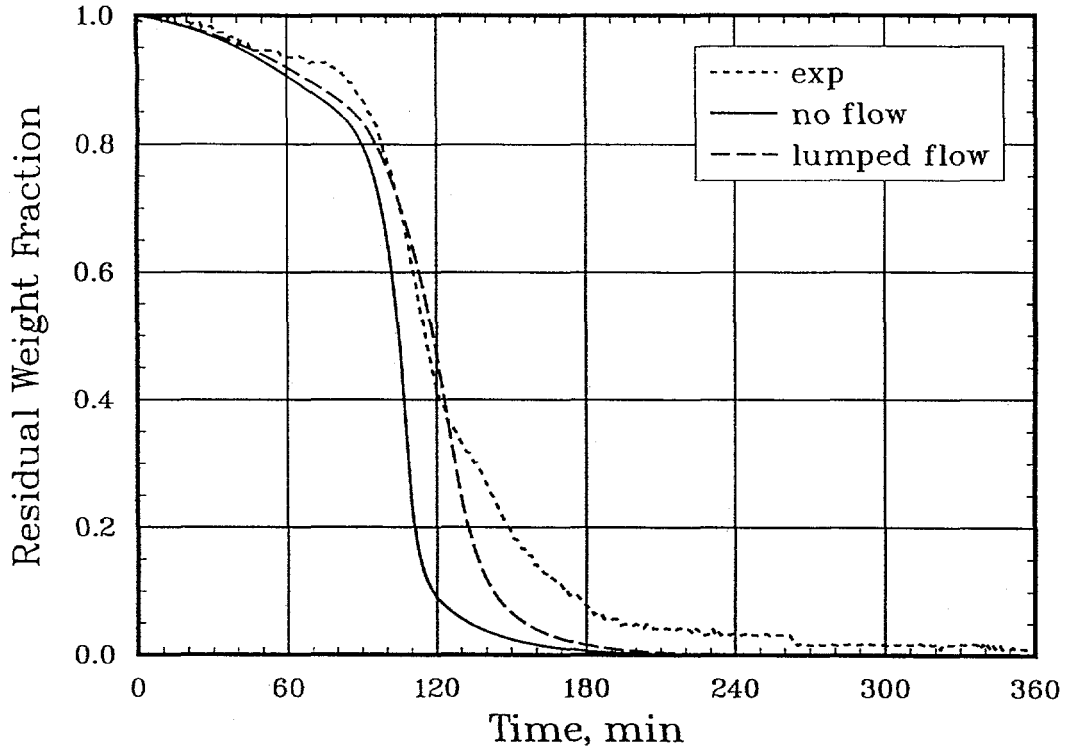

Figure 5. Measured residual weight fraction of binder with time, while heating with 50 W constant power, in comparison to the predictions of the no-flow and lumped-gas flow binder burnout computer models.

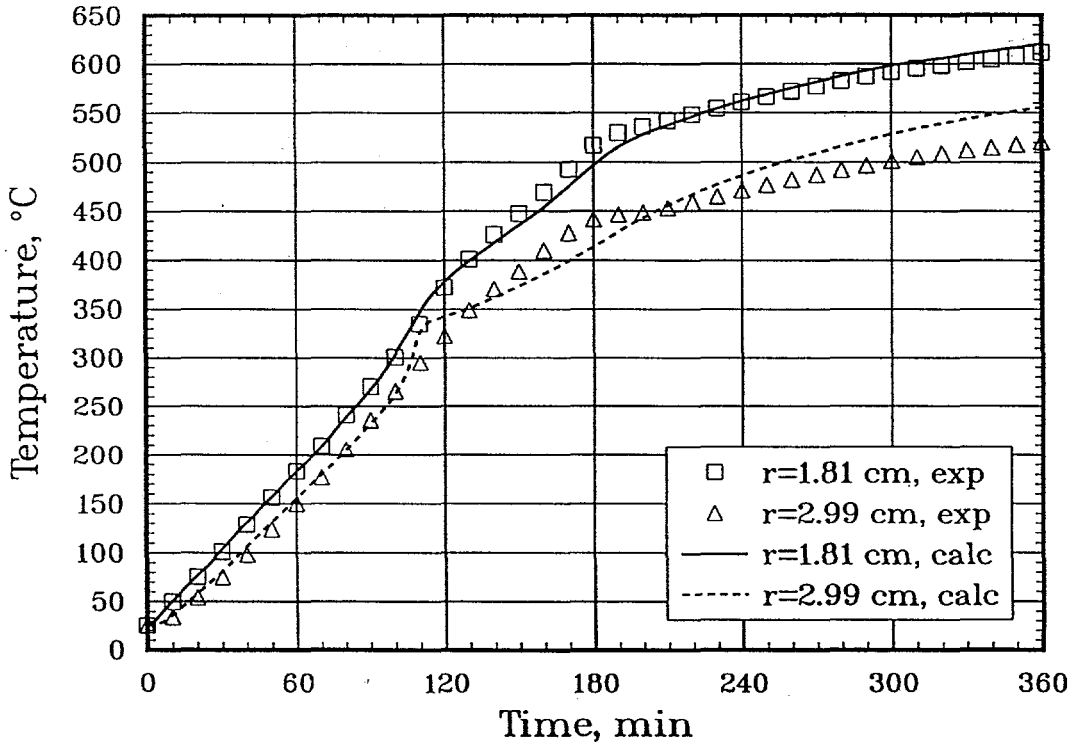

Figure 6. Measured temperatures with time at radial positions r = 1.81 and 2.99 cm in the center of a green ceramic stack heated with 50 W constant power, in comparison to the predictions of the no-flow model.

Table 1. Temperature dependent heat capacity and thermal conductivity of green and calcined alumina powder compacts pressed to ~65% relative density. Heat capacity was estimated [16]. Thermal conductivity was determined by tuning computer model parameters to replicate observed transient heat flow through pressed powder compacts.

Temperature, K	Heat Capacity, J/kg·K	Thermal Conductivity, W/m·K	
		Green	Calcined
273	724.3	0.674	0.362
333	839.7	0.635	0.342
373	902.5	0.609	0.328
453	1000.8	---	0.300
513	1053.5	---	0.279
573	1092.4	---	0.258
793	1177.0	---	0.182
953	1217.1	---	0.127
1173	1253.1	---	0.050

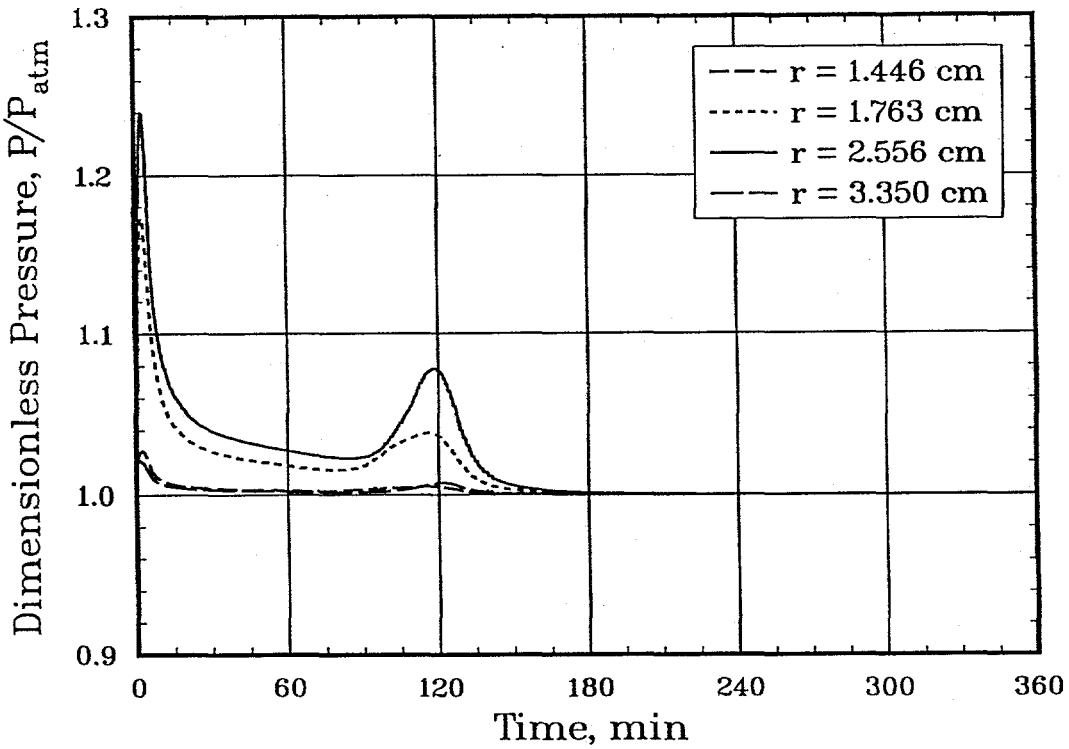

Figure 7. Predicted pressures with time at radial positions r = 1.444, 1.763, 2.556, and 3.350 cm in the center of a green ceramic stack heated with 50 W constant power.

binder burnout. The first peak pressure occurs within the first few minutes of heating, when the green powder compact is impermeable to gas flow, as gasses trapped within the closed pores in the compact expand with increasing temperature. The second peak occurs at ~120 min, as gas by-products evolve from the binder burnout reaction. Increasing the heating rate increases the absolute magnitude of both peaks, but the first peak is always the largest.

Likewise, the peak pressures are highest in the center of the powder compact. The results indicate that powder compact permeability is a critical parameter in binder burnout. Likewise an accurate description of powder compact permeability, and how it changes with time, will be crucial to model development and the accuracy of the data generated using the binder burnout models.

5. SUMMARY

A nominally one dimensional (1-D) prototype furnace has been designed to test, refine, and validate computer models that simulate binder burnout assuming a 1-D thermal gradient across the ceramic body during processing. Experimentally, 1-D radial heat flow was achieved using a rod-shaped heater that directly heats the inside surface of a stack of ceramic annuli surrounded by thermal insulation. Consistent with predictions from the control volume finite element method (CVFEM) thermal model used to design the furnace, experimental data show that relatively uniform radial heat flow is achieved during binder burnout. The detailed, precise, and highly reproducible data obtained using the prototype binder burnout furnace are being used to develop and refine computer models for binder burnout, and to conduct parametric studies to elucidate critical material property data required to support binder burnout model development.

The computational modeling effort focused on producing a macroscopic model for binder burnout based on continuum approaches to heat and mass conservation for porous media. Two increasingly complex models have been developed that predict the temperature and mass of a green powder compact as a function of time during binder burnout. The pressure within a powder compact during binder burnout also can be predicted with the more complex model. Model predictions are in reasonably good agreement with experimental data on binder burnout from a ~57 and 65% relative density pressed powder compact of a 94 wt% alumina body containing ~3 wt% binder. Results of the experimental studies are being used to test, refine, and validate the computational models.

6. REFERENCES

1) D. W. Richerson, "Powder Processing," pp. 374-417 in Modern Ceramic Engineering, second edition, Marcel Dekker, Inc. New York, 1992.
2) J. S. Reed, "Pressing," pp. 329-54 in Introduction to the Principals of Ceramic Processing, John Wiley & Sons, New York, 1988.
3) J. S. Reed and R. B. Runk, "Dry Pressing", pp. 71-93" in Ceramic Fabrication Processes, Treatise on Materials Science and Technology, **Vol 9**, edited by F. F. Y. Wang, Academic Press, New York, 1976.
4) D. W. Richerson, "Shape-Forming Processes," pp. 418-518 in Reference 1.
5) I. J. McColm and N. J. Clark, "Processing Stage 2- Greenbody Forming," pp. 141-207 in Forming, Shaping and Working of High Performance Ceramics, 1988.
6) D. W. Richerson, ed., "Forming and Predensification, and Nontraditional Densification Processes," pp. 123-241 in Engineering Materials Handbook, **Vol 4**, Ceramics and Glasses, ASM International, Materials Park, OH, 1991.
7) J. S. Reed, "Flocculants, Binders, and Bonds," pp. 152-73 in Reference 2.
8) T. Morse, Handbook of Organic Additives for Use in Ceramic Body Formulation, Montana Energy and MHD Research and Development Institute, Butte, MT, 1979.
9) D. W. Richerson, "Shape-Forming Processes," pp. 418-518 in Reference 1.
10) J. S. Reed, "Firing Processes," pp. 440-74 in Reference 2.